Building site investigation by joint shear wave reflection seismic and geotechnical drilling at Tønsberg hospital area, eastern Norway

U. Polom[1], J.S. Rønning[2,3], G. Tassis[2], J. Gellein[2] and G. Druivenga[4]

Introduction

In northern hemisphere countries such as Norway, Sweden, Finland, Russia, Canada and Alaska (USA), so called quick-clays seriously affect the safe building of settlements, and depth to bedrock is essential to know regarding safe building foundation. Such clays show a mineralogical structure where the stability is dependent on the ionic content in pore water. The composition is sensitive to leaching by low mineralized water. Originally deposited in a marine or brackish environment, clay formations composed of silt and clay are exposed to freshwater owing to the isostatic uplift of nearly 200 m (Bjerrum et al. 1967, ca. 180 m in our study area Tønsberg, www.ngu.no) above sea level after deglaciation. This may have caused leaching to low salinity depending on the time and volume of fresh water inflow, which may destabilize the formation up to a sudden liquefaction collapse. The detection of safe building ground e.g. bedrock and the knowledge of the internal soil structure above it is therefore essential in areas prone to quick-clay. Typically, quick-clays are not exposed to the surface and covered by other lithological units, which makes it difficult to map their area in the subsurface.

The administration of the central hospital of Tønsberg (Sykehuset I Vestfold, SIV), Norway, planned to expand the hospital with new buildings towards an area prone to quick-clay (Figure 1). Past borehole investigations indicated an undulating bedrock topography below soil, with clay, silt, and anthropogenic infills estimated up to 25 m thick and dense borehole grid was needed for accurate depth to bedrock knowledge. Ground Penetrating Radar (GPR) was tested, but failed owing to high electric conductivity in marine sediments. Geoelectric and electromagnetic methods previously applied in other locations by Long et al. (2012) and Solberg et al. (2016) were considered, but were discarded owing to lots of buried hospital infrastructure e.g. pipes, cables and underground transportation tunnels, and the disturbing urban environment. Seismic refraction could not provide the resolution required and was also limited in application owing to the restricted space, the nearby buildings and the asphalt pavement at the surface. Therefore NGU, as geophysical project leader, advised SIV to provide shear wave reflection seismic surveying prior to a focused drilling campaign. Because of the lack of competence of this research in Norway, NGU established a joint research expertise enabling the full range from shallow reflection seismic acquisition and geotechnical analysis towards geological model building for the construction site planning.

Site description

The investigation area is located at 21-28 m a.s.l. on the northern flank of the so called Castle Mountain, north of the Tønsberg city centre. The geological setting is part of the Oslo Graben

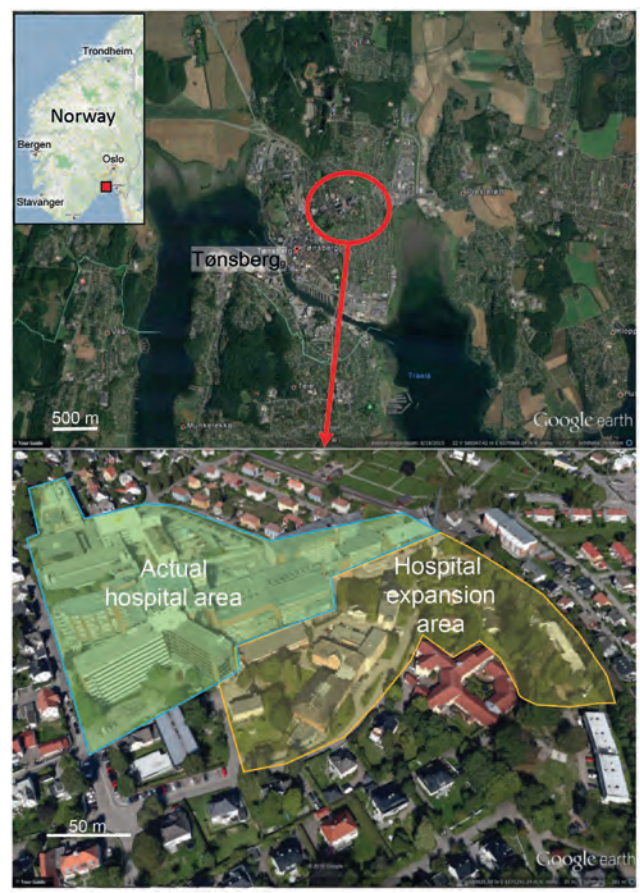

Figure 1 Map and satellite photos of the investigation site southeast of the SIV hospital near the centre of Tønsberg, Norway. Target of the investigation was the area planned for the hospital expansion, which is covered by older hospital buildings, parking lots, supply roads, residential buildings, hospital support buildings and roads.

[1] Leibniz Institute for Applied Geophysics, Germany | [2] Geological Survey of Norway, Norway
[3] Norwegian University of Science and Technology, Norway | [4] GEOSYM, Germany
[*] Corresponding author, E-mail: Ulrich.Polom@liag-hannover.de

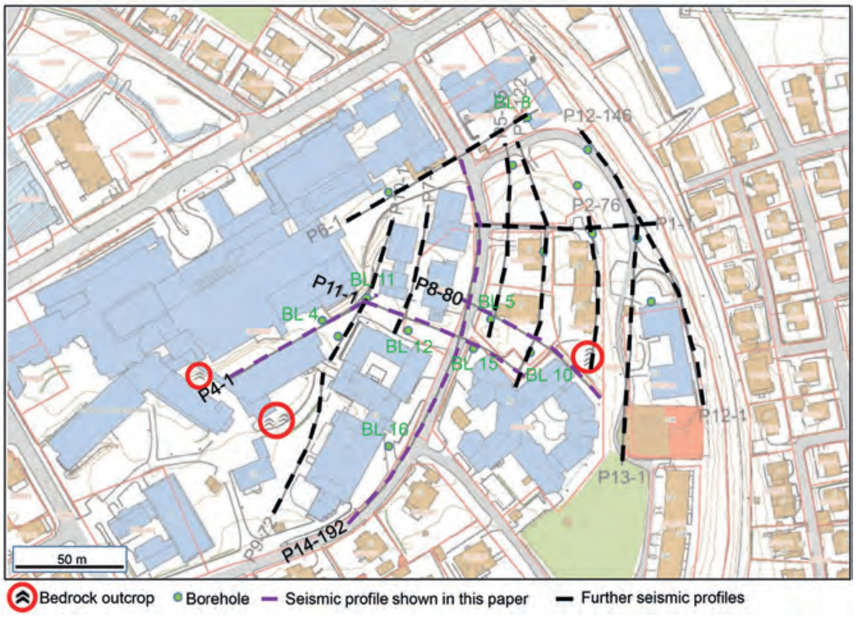

Figure 2 Seismic profiling grid (black lines, magenta lines referred in this paper), subsequently carried out reference boreholes (green dots) and bedrock outcrops (red circles).

Acquisition parameters	
Period:	6–11 June 2016
Instrument:	Geometrics Geode
Channels/rec:	71+ 1 aux
Seismic Source:	ELVIS version 3-S8 shear wave source system
Sweep type:	20-120 Hz linear, 10 s, 200 ms taper
Recording:	12 s , 2 s after correlation
Sampling int.:	1 ms
Recording filter:	off
Spread type:	variable split-spread
Geophone type:	SM6 H (10 Hz), single units mounted on GEOSYM land streamer system, or commonly planted in soil at non paved areas
Receiver interval:	1 m
Source interval:	2 m
Vertical stack:	2-fold[+Y]-[-Y] alternated vibrations
Total length:	1389 m
Total data:	4.36 Gb
No. of records:	1440

Table 1 Seismic acquisition parameters.

zone and shaped by young volcanic and magmatic activity. The main rock formation in the area is rhobus porphyry (www.ngu.no), which is the bedrock formation expected at the investigation site, also observed at some outcrops in the area. During glaciation the area was below sea level, where marine sedimentation of sand, silt, and clay took place. After deglaciation the area was isostatically uplifted ca. 180 m (www.ngu.no) above sea level. Drilling investigations in the neighbourhood prior to the seismic survey detected a strong varying bedrock topography below clay, silt, sand, including boulders, and anthropogenic infills (Aarset, personal communication). The sediment thicknesses was estimated up to 25 m, whereas the range of the sediment thickness and internal structure was widely unknown.

The surface at the investigation site is partly covered by the main buildings of the hospital in the northern part and additional hospital support buildings in the southern and western part of the area, the space in between is used for supply logistics roads and parking lots. In the underground infrastructure pipes, cables and underground transportation tunnels for building supply logistics and communication are installed. In the eastern part, five small residential houses surrounded by small garden areas were present, the area was also partly planned for new hospital buildings during the hospital expansion. The eastern border of the planned expansion area adjoins a railway frequently in use, which travels around the hill.

Method – survey design, seismic data acquisition and processing

Based on successful shallow shear wave reflection surveys in the harbour area of Trondheim, Norway, (Polom et al., 2010; Hansen et al., 2013; L'Heureux et al., 2013), experimental quick-clay investigation sites in southern Norway (Sauvin et al., 2014) and southern Sweden (Malehmir et al., 2013; Polom et al., 2013), shallow shear wave reflection seismic has been shown to be a proven technique to solve this difficult task. Pugin et al. (2013) also referred to the applicability of the method over quick-clays in Canada. A 72-channel land streamer system and an ELVIS vibrator (Krawczyk et al., 2012) source solved the subsurface access limitations on the surface. In the case of a non-paved surface, the land streamer receiver array was supplemented by planted geophones. At project start, the main difficulties were the sparse knowledge of the depth-to-bedrock and the expected man-made infills during the past, which hampered a target-oriented acquisition design. Whereas quick-clays are usually of low shear wave velocities (below 150 m/s) requiring short midpoint spacing of nearly 0.25 m, infills, glacial overprints and surface pavement were expected to significantly raise the average shear wave propagation velocities above the bedrock. Therefore, the final survey design was decided after tests on site to 0.5 m midpoint spacing (1 m geophone spacing) and 2 m source interval in general, resulting in an average common midpoint (CMP) coverage of 18-fold. The source signal (sweep) was set to 20-120 Hz linear of 10 sec duration, two recordings with alternating polarity were carried out at each source location. Data was stored uncorrelated to enable detailed noise editing later on, if required. In joint planning with SIV, the area of interest was covered by a dense grid of 14 profiles (1360 m total) adjusted to the conditions at the surface on site (Figure 2).

Seismic data was acquired on 6-11 June, 2016 by a three-member field crew of NGU and GEOSYM (Figure 3), with recording parameters listed in Table 1. Most of the profiles were acquired in daylight, but avoiding the rush hours of the hospital. Since the hospital machinery is commonly operating 24 hours a day, the noise level around the buildings was nearly the same during day and night. Profile 14 was acquired on a public road at night time supported by a temporary road closure. Every day the production data was transmitted online to the processing office at LIAG in Hannover, Germany, for quality control and initial data processing. Parallel to the profiling, DGPS positioning of the profiling was carried out, sometimes impaired by low satellite coverage caused by satellite shadowing by to the hospital buildings. Accuracy of shot and geophone elevation were later improved using LIDAR data with height resolution of 1 dm and five points per m^2 (Data provided by Norwegian Mapping Agency, Statens Kartverket).

It was proposed to apply reflection seismic data processing in a two-stage operation for all profiles. An initial stage should produce a first raw subsurface image grid to define appropriate borehole locations for bedrock depth evaluation in the area, as early as possible. In a second stage the initial seismic results should be adjusted and fine-tuned to the borehole results, especially regarding the expected S-wave velocity assignment uncertainty. Whereas such velocity uncertainty is of low significance during the time domain processing sequence, depth errors were expected, especially in the final time-to-depth conversion step.

The initial reflection seismic data processing run was carried out using a standard processing sequence (Krawczyk et al., 2012; Polom et al., 2013; Pugin et al., 2013) applied to all profiles (Table 2), including small individual adaptions. During the data processing it was observed that the data from the eastern part of the area show partly very shallow (a few metres refractor depth estimated) SH-wave refractions of very high velocity (> 2500 m/s), indicating a shallow bedrock contact. This was supported by a lack of high amplitude reflections, which were expected at the sediment-to-bedrock interface. This observed effect changed towards the western part of area, where the occurrence of shallow refractions was degraded and strong reflections occurred.

Based on the initial seismic results, a pattern of 17 boreholes was designed within the seismic profile grid. Subsequently, the boreholes were carried out by the geotechnic contractor Multiconsult (Raen 2016), until depth of bedrock for sediment lithology analysis, structure matching and depth verification (Figure 2). To analyse sediment stratification, mechanical soil parameters and pore pressure conditions, Cone Penetration Test with pore pressure measurements (CPTU) and Piezometer were used. Positioning of the boreholes were carried out using DGPS. In the following, results of boreholes and the seismic profiling grid were joint interpreted in 2.5D to perform a depth-to-bedrock horizon, which was finally modified to a 3D bedrock surface.

Results

Figure 4 shows shot gather examples acquired along profile 14, which was carried out on a public road near the centre of the

Reflection seismic data processing
1. Vibroseis correlation (using the recorded pilot sweep)
2. Bad trace elimination
3. Vertical stack (2 records at each source location)
4. Geometry assignment (crooked line binning)
5. Amplitude scaling (AGC 220 ms)
6. Bandpass filter (18-22-105-115 Hz)
7. CMP sort
8. Interactive velocity analysis
9. Normal moveout correction
10. CMP-stack
11. Trace energy normalization
12. Finite difference (FD) time migration
13. Time-to-depth conversion (using derived RMS stacking velocities)
14. Elevation statics to 28 m a.s.l.

Table 2 Generalized reflection seismic processing sequence applied to the data.

Figure 3 Photo impressions of seismic surveying: a) at profile 4, showing the wheelbarrow-based shear wave vibrator source, b) at profile 11, c) at profile 10 and d) at profile 3. Since most of the investigation area is paved by asphalt and concrete a land streamer configured to 1 m receiver interval was the preferred receiver system. In b) unused parts left in bows.

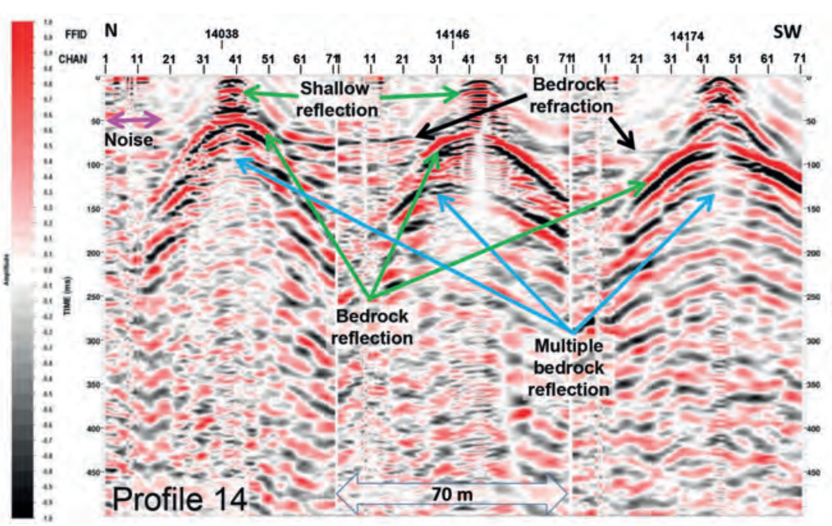

Figure 4 Examples of shot gather records from profile 14 (AGC 220 ms and Bandpass Filter 18-22-105-115 Hz applied) showing the varying response of the subsurface wave propagation. The bedrock reflection amplitude is the strongest event of nearly 200 m/s RMS velocity, followed by the multiple bedrock reflection, which is obviously surface reflected in the FFID 14038 and FFID 14146, and interbed reflected in FFID 15174. At the bedrock interface a refracted SH-wave of nearly 2800 m/s was generated, indicating very stiff bedrock material. Above the bedrock very shallow reflections of the sediment cover are visible. Note the complete absence of air blast and Love surface waves in the records.

profiling grid. Owing to its position within the grid, its length and relative good bedrock reflection response, it could be used as a marker profile to parameterize and to evaluate the data processing sequence. The records along the profile show shallow reflections from interfaces within the sediment layers above the bedrock, a strong bedrock reflection event of well-defined hyperbola curvatures, a bedrock-surface-bedrock multiple reflection of similar precise shape and a high-frequency refraction response that propagated along the top bedrock interface. The analysis of the bedrock reflection hyperbola shape yields to nearly 200 m/s RMS (Root mean Square) S-wave velocity, whereas the attached refraction event shows nearly 2800 m/s S-wave velocity at the top of the bedrock. Applying these velocities in Snell's law, the minimum angle of incident for refraction into the bedrock layer is to 4.1 degrees. Therefore, this kind of bedrock refraction can be expected along the whole receiver spread in the area and can be used as an additional indicator for the bedrock contact. Owing to the surface pavement of asphalt and the road construction, direct waves are of low amplitude only as a result of the stiff surface. Love surface waves are completely suppressed by the inverse velocity gradient at the surface. This condition also hampers the detection of a layer 1 velocity regarding a common refraction analysis. No air blast contamination disturbs the records, only channels 1-11 are slightly affected by noise, induced probably by electromagnetic fields in the area.

Figure 5 shows the resulting depth section of profile 14 after the initial processing using the sequence shown in Table 2. The final elevation datum was set to 28 m a.s.l. with respect to the maximum elevation in the investigation area. The section images all reflection elements already visible in the shot gathers, with depth adjustment being based on RMS velocities derived from hyperbola shape only. Regarding the bedrock depth detected in borehole BL16 (3.9 m distance to the profile track) subsequent to the seismic imaging, the signature of the bedrock contact was marked at the end of the positive (red) bedrock reflection amplitude for further interpretation. In the north, the bedrock is detected nearly 5 m below the surface, the sediment cover above shows only weak internal structures. From the position of borehole BL 15 towards southwest the bedrock dips towards 11 m below surface. The image of the sediment cover above shows boundaries from the infill to the silt-clay layer and from the silt-clay layer to the sand layer. A bedrock surface multiple reflection is observed along the entire profile as well as internal bedrock structures.

Shot gather examples of the crossline profile 11 in Figure 6 show an inclining bedrock reflection from northwest to southeast, which is also supported by the apparent S-wave refraction velocities (too fast in record 11002: 7200 m/s, too slow in record 11080: 1030 m/s) of the bedrock. In record 10080 the bedrock is already too close to the surface to generate a distinct bedrock reflection event regarding the receiver set-up used. The nonlinearity of the bedrock refraction event indicates a ragged bedrock surface. The data traces near to NW are contaminated by noise generated

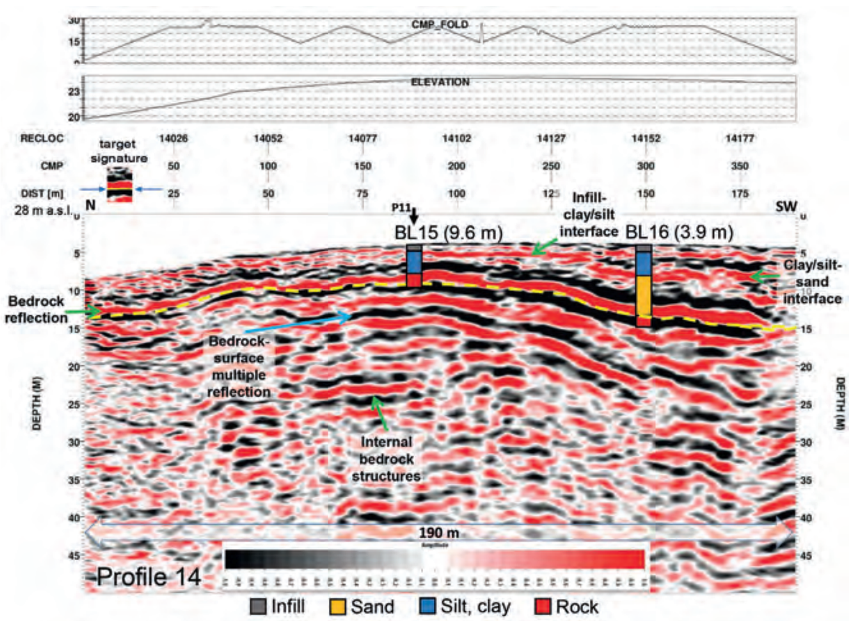

Figure 5 Depth section of profile 14 (depth converted post-stack FD time migration, referred to 28 m a.s.l.) along the road in the centre of the investigation area and included blocked borehole lithology. Numbers in brackets beside the borehole names denote perpendicular borehole offsets to the profile. The bedrock interface (dashed yellow line) is clearly imaged along the profile showing a constant target signature referred to the lithology in borehole BL16. A very shallow reflection nearly 2 m in depth between BL 15 and BL16 indicates the infill-clay/silt interface, a further reflection in the SE part indicates the clay/silt-sand interface in BL 16. Deeper reflection events – except the bedrock-surface multiple- show internal bedrock structures. The depth section based on derived RMS reflection velocities only without depth adaption to the boreholes carried out after the seismic survey. The joint position to profile 11 is marked by a black arrow on top.

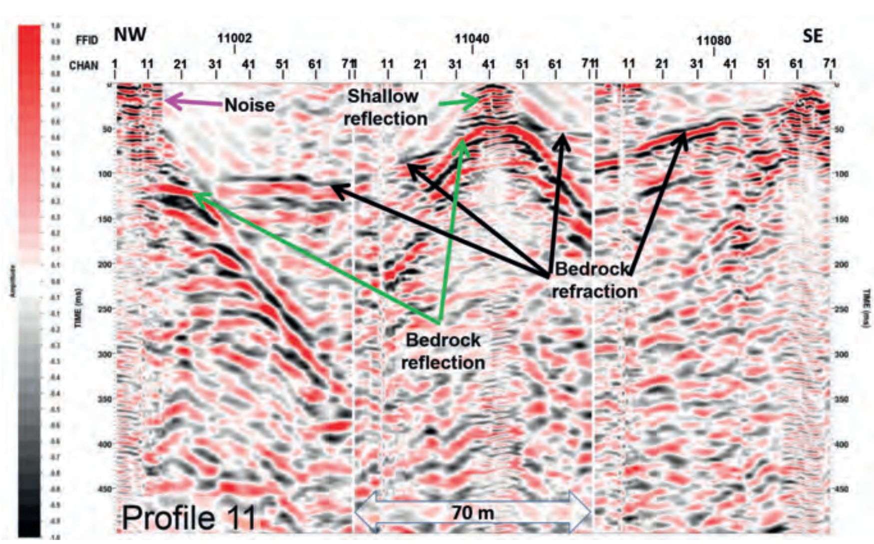

Figure 6 Examples of shot gather records from profile 11 (AGC 220 ms and Bandpass Filter 18-22-105-115 Hz applied). In records 11002 and 11040 the bedrock reflection hyperbola is clearly imaged and moving upward in time. The bedrock reflection is coupled to a bedrock refraction event which shows apparent refraction velocities of 7200 m/s in record 11002 and 1030 m/s in record 11080, indicating a NW dipping bedrock surface. Above the bedrock only weak shallow reflections of the sediment cover are visible. Data traces in the northwest part are almost affected by engine noise generated randomly inside the hospital building.

inside the main hospital building (see Figure 2). The resulting depth section (data processing with respect to Table 2) in Figure 7 clearly images the nearly 30 degree northwest dipping bedrock, which is also proved by the reference boreholes carried out later on. The dip is not continuous, there are two interruptions visible at positions of boreholes BL 12 and BL 11. The interface between the silt-clay layer and the sand layer is not clearly imaged, while the image of the upper interface between infill and the silt-clay layer is weak.

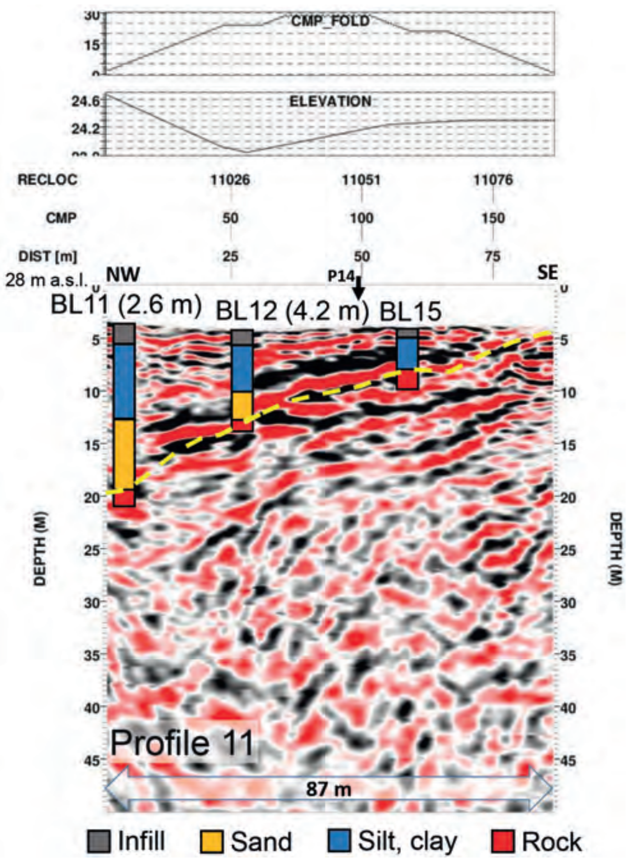

Figure 7 Depth section of profile 11 (for processing status see Figure 5) imaging a NW dipping, obviously discontinuous bedrock reflection, which sufficiently fits the lithology detected in the boreholes carried out subsequently. The joint position to cross profile 14 is marked by a black arrow on top.

Figure 8 shows shot gather examples of profile 4, which is closely situated and parallel to the main hospital building (Figure 2). West of the profile the bedrock outcrops at the surface. The record examples show an obviously northeast-dipping bedrock owing to the low apparent refractor velocity in record 4002, where the bedrock reflection is hardly visible. Record 4048 in the centre of the receiver spread shows a clear bedrock reflection with shifted hyperbola apex to the southwest in relation to the shot position, indicating a slightly northeast-dipping reflector. All records of this profile are contaminated by strong noise from inside the hospital building, visible for example in record 4076, where no clear bedrock reflection can be detected. Additionally, it is hard to identify any indication of a boundary in the sediment layers above the bedrock reflection.

Because of the high noise contamination, the depth section of profile 4 in Figure 9 is of less imaging quality compared to the profiles 11 and 14 (Figures 7 and 5). Without a reference from a borehole, a distinct interpretation of a bedrock reflection is not possible, only a structural dip of nearly 30 degrees towards northeast is visible. Furthermore, there is no clear indication about boundaries in the sediment cover above the bedrock. With respect to the refractor indications in the shot gather records (e.g. record 4002) in Figure 8, the bedrock needs to be shallower to the surface in the southwest than it is imaged in the depth section. It is obvious from the reflector imaging that the bedrock surface is cragged along this profile.

The depth section of profile 8 in Figure 10 shows an example for a profiling result above very shallow bedrock in the investigation area. Additionally, the surface was only partly paved along the profile track, so planted geophones were used additionally to the land streamer to improve the seismic coupling. Borehole BL10 detected compact bedrock at 0.9 m below the surface, borehole BL5 detected weak and broken bedrock at 2.5 m below surface. Between the boreholes, at a distance of nearly 25 m, the bedrock structure in the seismic section images a antiform, which nearly touches the surface. The detection capabilities for the sediment boundaries by the reflection method above such shallow bedrock depth is out of the resolution range for the equipment set-up used. Comparing the reflection pattern of the bedrock along the profile and the lithology from boreholes indicate

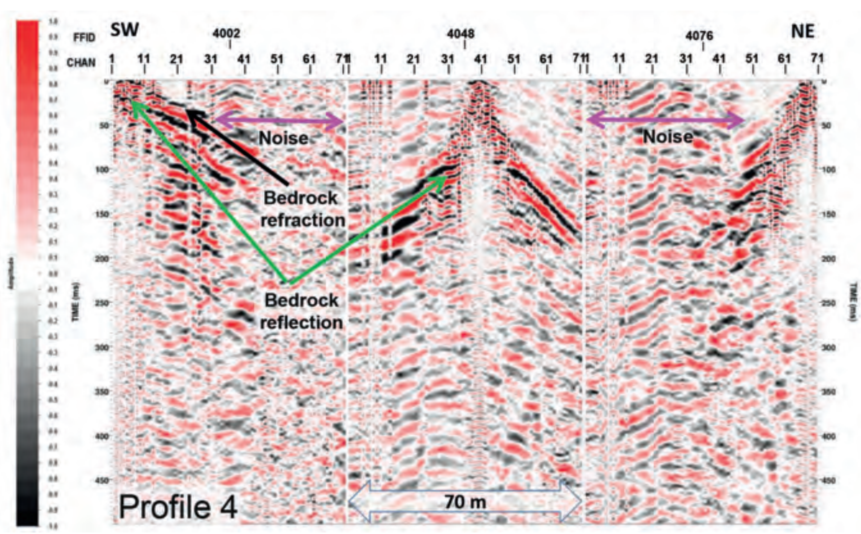

Figure 8 Examples of shot gather records from profile 4 (AGC 220 ms and Bandpass Filter 18-22-105-115 Hz applied). Owing to the close and parallel location to the main hospital building the data of this profile is widely contaminated by noise (ranges denoted by magenta arrows) from continuous running machinery inside the building. Nevertheless, some records in the centre part of the profile (here as example record 4048) clearly image the bedrock reflection along short source-receiver distances (offsets).

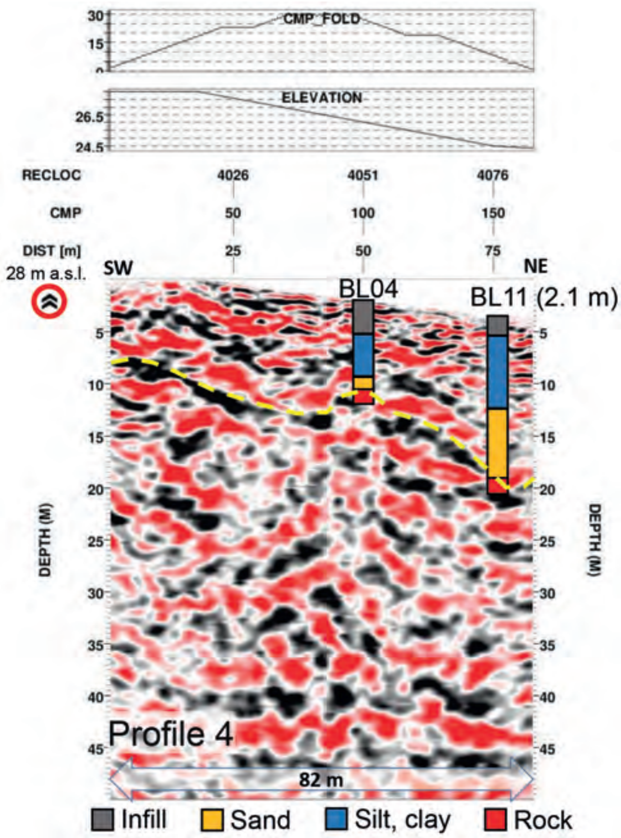

Figure 9 Depth section of profile 4 (for processing status see Figure 5) imaging a NE dipping bedrock reflection structure. A location of outcropping bedrock is denoted SE of the profile. Owing to the high noise contamination bedrock interpretation strongly benefits from evaluation boreholes.

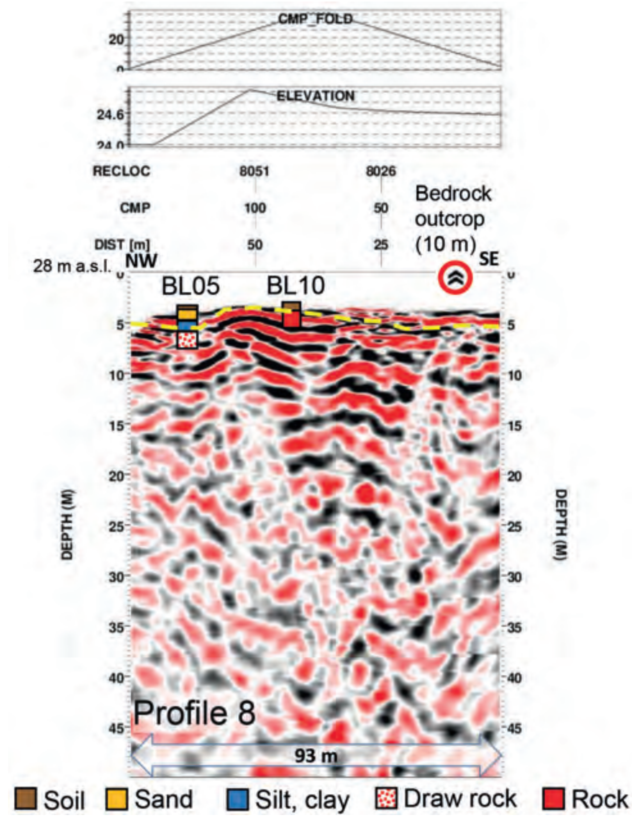

Figure 10 Depth section of profile 8 (for processing status see Figure 5) as an example for profiling locations where the bedrock was detected by boreholes only 0.5-2 m below the surface. In these cases the profiling set-up mostly failed to resolve the bedrock surface and the sediment structures above by the reflection method. Additional application of the refraction method would have achieved an improved bedrock imaging, but was not required with respect to the aim of the investigation.

strong variations in the top bedrock material quality along short distances . The bedrock outcrop in the southeast of the Profile 8 with 10 m offset to northeast is not indicated in the seismic image.

After initial data processing and cross-check of depth sections and boreholes in the 2D sections, only small deviations were found for the depths to bedrock, with respect to the final remaining surface elevation error of +/- 0.5 m. Therefore, all profiles and boreholes were imported into a 3D interpretation system for a comprehensive bedrock horizon analysis, neglecting the original intention of an additional processing run to optimize the depth sections after the borehole campaign for final interpretation. Within the 2.5D grid of seismic sections referenced by the bedrock depths detected in the boreholes, the bedrock horizon surface was interpreted and subsequently interpolated in 3D, to enable a widely consistent solution in an iterative run. Owing to a lack of sufficient gridding algorithms and to also include the information about bedrock outcrop location, the final depths to bedrock below surface were exported for each profile and gridding was carried out using SURFER software.

Figure 11 shows a scene of the 3D image from the interpretation system including seismic profiles 14 and 11, depth of top bedrock detected by boreholes, the picked 2D horizons along the seismic profiles, and the simplified 3D horizon of top bedrock and surface in a vertical-to-horizontal relationship of 5:1. It indicates an upper shelf of the bedrock in the southeast with only few metres sediment cover and a steep bedrock syncline of up to 17 m sediment cover in the northwest of the investigation area.

Figure 12 shows the final gridded maps of the bedrock topography relative to sea level (a) and soil thickness below surface (b) derived from the combined 3D interpretation of seismic sections and boreholes including the bedrock outcrop locations. The maps image the strong varying bedrock topography and the sediment cover above in the investigation area in detail, showing the coherent upper shelf area in the east. A southwest-northeast trending bedrock valley of minimum 10 m sediment cover is aligned in the northwest including a syncline maximum of 17 m sediment cover directly beside an edge of the main hospital building.

Figure 13 shows a 3D image of the bedrock topography above sea level giving an impression of the strong variations in bedrock depth below the surface in a small area about 230 m east and 180 m north. Whereas the areas of shallow bedrock in the southeast are mostly covered by thin layers of infill and soil, the deeper bedrock areas along the bedrock valley are mainly filled by sands and clay-silt layers of up to 8 m thickness each (Figures 5, 7, 9), covered at top by infills of several m thickness.

Discussion

In the southeast part of the investigation area the bedrock was detected at only 0.5-3 m below the surface, whereas in the northern and western part the sediment cover reached a thickness of up to 17 m. In the shallow bedrock area in the southeast, the seismic imaging of the top bedrock and the sediment structures above it were weak in general, probably also because of man-made infills at the surface above the clay layer which was reported during reference drilling. In these areas the aperture of the seismic receiver set-up used was too large to achieve a sufficient reflection image, most of the S-wave energy propagated along refraction paths at the top of the bedrock and as Love waves in the shallow low velocity layers above the bedrock. Additional use of refraction tomography in this area would probably have improved the resolution of the bedrock topography, but this additional data analysis was not required in terms of foundation design owing to the shallow bedrock there. Additional application of surface wave inversion by using the Love wave dispersion was in general estimated to be critical since the layering in the whole area does not meet the requirements of an approximated 1D situation (e.g. Figure 6). Such surface wave analysis was also hampered by the surface pavement and the shallow infill material, which strongly affected the Love wave propagation due to velocity inversions near the surface.

Data quality was evaluated to be good along six profiles, moderate along two and poor along six profiles (Rønning et al., 2016). Good data quality were achieved mostly in areas with asphalt-paved roads while bad quality appeared in grass-covered areas, probably with infill material and low depth to bedrock. Normally, carrying out geophysics in urban areas on asphalt the data quality is reduced. with the shear wave method used here, data quality benefits from asphalt and low noise and no destructions during data acquisition makes the method superior in urban areas.

Clear and strong bedrock reflection images could be achieved at depths of more than 4 m, the best data quality was achieved along profile 14 (Figure 5) also owing to the continuous surface pavement of asphalt along a public road. Since the depth section of the initial processing run for profile 14 fitted the depth of the evaluation borehole BL 16 carried out later on, this profile was used as a master profile for the whole survey with respect to the processing sequence used and to build up the interpretation grid for horizon analysis. Based on the tie points of the profiles and the borehole pattern the interpretation could be continued successfully along the whole investigation area. Only a few interpretation problems remained in the southeast area owing to a lack of borehole coverage. Nearly all of the evaluation borehole fit the

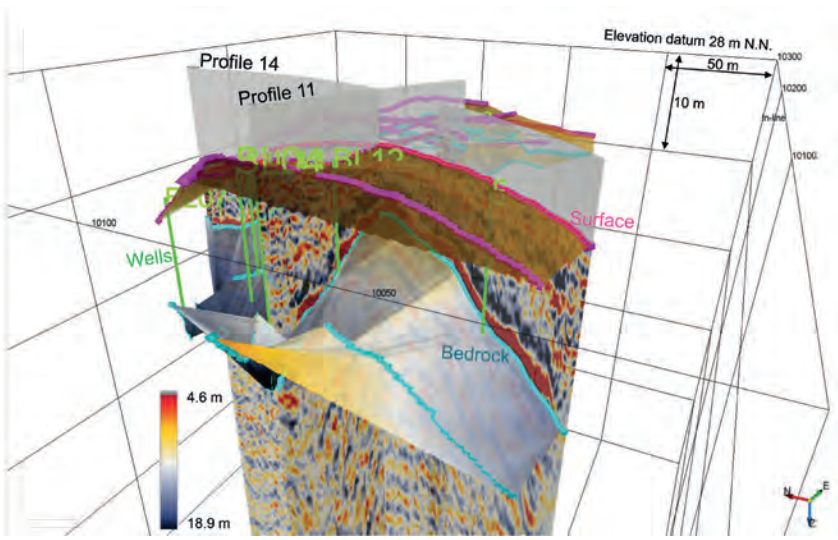

Figure 11 Scene of the joint interpretation of the 2.5D seismic profiling grid and reference boreholes (in green, borehole bottoms show bedrock level) showing the surface topography and the interpolated bedrock horizon (both colour coded elevation). Light blue lines show interpreted top of bedrock, magenta lines image the surface topography.

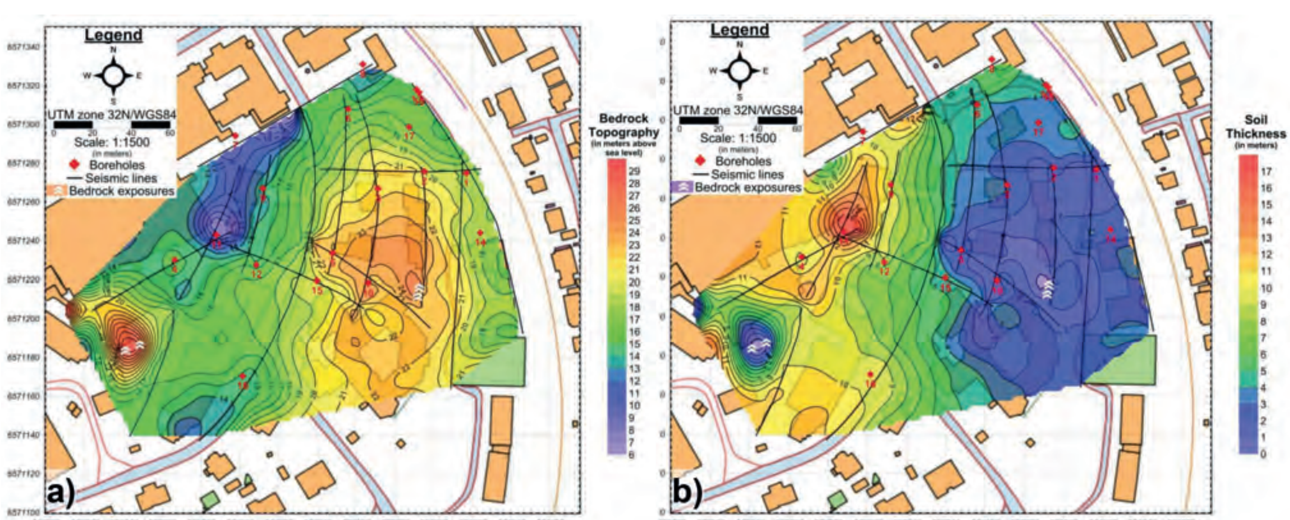

Figure 12 Resulting maps of bedrock topography above sea level (a) and sediment thickness above bedrock (b). Beside the joint interpretation of seismic and boreholes the maps include outcrop manifestations at the surface, where boreholes and seismic profiling could not be realized. The maps provide a comprehensive basis for the selection of building foundation types required in the hospital expansion area, supporting an efficient construction planning management.

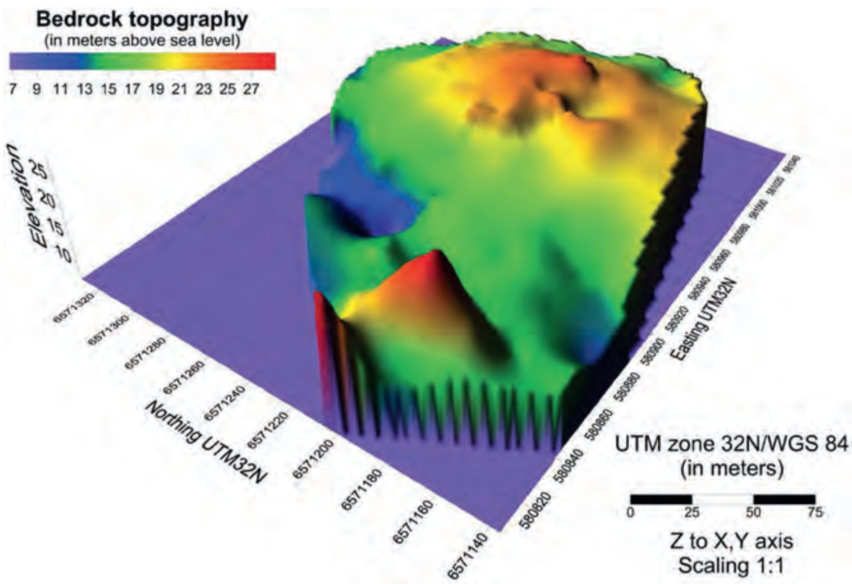

Figure 13 Derived bedrock topography in a 3D image referenced to sea level elevation showing the overall dualistic situation. Whereas the bedrock forms a horst structure very shallow to the surface in the eastern part, a valley structure including two deep local synclines filled with marine sediments dominates the western part. The bedrock peak in the foreground resulted mainly from a local outcrop manifestation, which prevented this area from being covered by seismic profiles and boreholes during the survey.

seismic images within +/- 0.5 m, which was also the uncertainty range of the DGPS elevation surveys of boreholes and seismic. BL8 at the northern end of the survey (Figure 2) was suspected to have met a rock boulder instead of the bedrock since it shows the only notable misfit discrepancy occurred, of nearly 10 m, between seismic bedrock image and borehole result.

For final interpretation and map generation the DGPS elevation results of boreholes and seismic were optimized later on by use of a LIDAR-based digital elevation model to further reduce the uncertainty range with respect to the final calculations for building foundations. Interfaces between clay and sand layers above the bedrock could partly be imaged (e.g. Figure 5), but show mostly a diffused and scattered seismic response (e.g. Figure 9). These interfaces would not have been detected without the borehole references. The internal bedrock structure shows a significant tectonic overprint beside the expected glacial erosion at the top.

In nearly all of the evaluation boreholes the clay and silt layer, which is prone to liquefaction, was found either underlain by sand or in direct bedrock contact. This situation supports the vulnerability to quick-clay leaching by freshwater at the bottom of the layer provided by fault pathways in the bedrock. The final interpretation of the depth-to-bedrock layer benefited from seismic and borehole results as well as surface outcrops.

The foundations of new buildings in the southeast part were expected to be investigated with small effort. In the northwest area, close to the existing hospital buildings, the subsurface situation requires increased effort of foundation construction owing to a sediment cover of 10 m and more, and a >16 m deep hole in the bedrock topography.

The high building density, which only allowed a few metres for operation, posed the most challenging tasks for seismic, drilling and precise geodetic surveying resulting in a final depth-to-bedrock uncertainty of +/- 0.5 m.

Conclusions

Despite the surprisingly difficult and unexpected subsurface and environmental conditions regarding undisturbed wave propagation in the subsurface and an equally difficult target geometry, the challenging mission to map the bedrock topography in the hospital expansion area was accomplished successfully. This result benefited mainly from the close combination of shallow high–resolution seismic with geotechnical borehole investigation, which enabled precise depth referencing of the top bedrock and its expansion in the area of interest. Even though some questions still remain unanswered, this experimental project highlighted the capabilities of combining geophysical and drilling methods, supported by surface outcrops.

Acknowledgements

Boreholes and geotechnical analysis was carried out by Multiconsult BV, Nedre Skøyen vei 2, 0276 Oslo, reported by Tracey Raen and Hans Ole Haugen. We would especially like to thank Sykehuset i Vestfold (SIV) and SIV project leader Inge Vidar Aarset for their support in proving this unique experimental investigation set-up in Scandinavia for the first time. We also gratefully acknowledge SIV for permission to publish the data and Inger-Lise Solberg (NGU) and David Colin Tanner (LIAG) for constructive comments to the manuscript.

References

Bjerrum, L. [1967] Engineering geology of Norwegian normally-consolidated marine clays as related to settlements of buildings. *Geotechnique* **17**, 81–118.

Hansen, L., L'Heureux J-S, Sauvin, G., Polom, U., Lecomte, I., Vanneste, M., Longva, O. and Krawczyk, C.M. [2013]. Effects of mass-wasting on the stratigraphic architecture of a fjord-valley fill: Correlation of onshore, shear-wave seismic and marine seismic data at Trondheim. Norway. *Sedimentary Geology,* **289**, 1–18.

Krawczyk, C.M., Polom, U., Trabs, S. and Dahm, T. [2012]. Sinkholes in the city of Hamburg – New urban shear-wave reflection seismic system enables high-resolution imaging of subrosion structures. *Journal of Applied Geophysics*, **78**, 133-143, doi:10.1016/j.jappgeo.2011.02.003.

L'Heureux, J-S., Long, M., Vanneste, M., Sauvin, G, Hansen, L., Polom, U., Lecomte, I., Dehls, J.F. and Janbu, N. [2013]. On the prediction of settlement from high-resolution shear-wave reflection seismic data: The Trondheim harbour case study, mid Norway. *Engineering Geology,* **167**, 72–83.

Long, M., Donohue, S., L'Heureux, J-S., Solberg, I-L., Rønning, J.S., Limacher, R., O'Connor, P., Sauvin, G., Rømoen, M. and Lecomte, I. [2012]. Relationship between electrical resistivity and basic geotechnical parameters for marine clays. *Can. Geotech. J.*, **49**, 1158–1168.

Malehmir, A., Bastani, M., Krawczyk, C.M., Gurk, M., Ismail, N., Polom, U. and Person, L. [2013]. Geophysical assessment and geotechnical investigation of quick-clay landslides – a Swedish case study. *Near Surface Geophysics*, **11**, 341–350.

Polom, U., L'Heureux, J.-S., Hansen, L., Lecomte, I., Longva, O. and Krawczyk, C.M. [2010]. High-resolution SH-wave reflection seismics for characterization of onshore ground conditions in the Trondheim harbor, central Norway. In: R.D. Miller, J.D. Bradford and K. Holliger (eds.), *Advances in Near-Surface Seismology and Ground-Penetrating Radar*, SEG, Tulsa, 297-312.

Polom, U., Bagge, M., Wadas, S., Winsemann, J., Brandes, C. and Krawczyk, C.M. [2013]. Surveying near-surface depocentres by means of shear wave seismics. *First Break*, **31** (8), 63-75.

Pugin, A.J.M., Brewer, K., Cartwright, T., Pullan, S.E., Perret, D., Crow, H. and Hunter, J.A. [2013]. Near surface S-wave seismic reflection profiling – new approaches and insights. *First Break,* **31** (2), 49-60.

Sauvin, G., Lecomte, I., Bazin, S., Hansen, L., Vanneste, M. and L'Heureux, J-S. [2014]. On the integrated use of geophysics for quick-clay mapping: The Hvittingfoss case study, Norway. *Journal of Applied Geophysics,* **106**, 1–13.

Raen, T. [2016]. *The Tønsberg project – Ground investigations. Multiconsult Geotechnical data report.* Document code 129172-1-RIG-RAP-001 (in Norwegian).

Rønning, J.S., Polom, U., Druivenga, G., Gellein, J. and Tassis, G. [2016]. *Ground investigations at the Hospital Property in Tønsberg.* NGU Report 2016.042 (in Norwegian). http://www.ngu.no/upload/Publikasjoner/Rapporter/2016/2016_042.pdf

Solberg, I-L., Long, M., Baranwal, V.C., Gylland, A.S. and Rønning, J.S., [2016]. Geophysical and geotechnical studies of geology and sediment properties at a quick-clay landslide site at Esp, Trondheim, Norway. *Engineering Geology*, **208**, 214 - 230 doi: 10.1016/j.enggeo.2016.04.031.